*Laser and Particle Beams*

**cambridge.org/lpb**

# Improved yield and control of spectra from high-intensity laser-generated neutron beams

Brian J. Albright, Lin Yin and Andrea Favalli

Los Alamos National Laboratory, Los Alamos, New Mexico 87545, USA

**Original Study**

**Cite this article:** Albright BJ, Yin L, Favalli A (2018). Improved yield and control of spectra from high-intensity laser-generated neutron beams. *Laser and Particle Beams* **36**, 15–21. https://doi.org/10.1017/S0263034617000908

Received: 22 May 2017
Accepted: 26 November 2017

**Key words:**
Deuterons; high-intensity lasers; ion acceleration; neutrons; relativistic-induced transparency

**Author for correspondence:**
Brian J. Albright, Los Alamos National Laboratory, Los Alamos, New Mexico 87545, USA. E-mail: balbright@lanl.gov

**Abstract**

Kinetic modeling of laser-ion beam generation from the "break-out afterburner" (BOA) has been modeled for several deuteron-rich solid-density target foils. Modeling the transport of these beams in a beryllium converter shows as much as a fourfold increase in neutron yield over the present state of the art through the use of alternative target materials. Additionally, species-separation dynamics during the BOA can be exploited to control the hardness of the neutron spectra, of interest for, for example, enhancing penetrability in shielded material in active neutron interrogation settings.

## Introduction

Short-pulse laser neutron sources [see, e.g., (Alvarez *et al.*, 2014) and references therein] enable compact neutron pulses suitable for a variety of applications, including fusion materials properties (Perkins *et al.*, 2000), biological studies (Zaccai, 2000), condensed matter physics (Ma *et al.*, 2013), detection of contraband non-nuclear (Buffler, 2004), and nuclear material (Favalli *et al.*, 2009, 2016*a*). Two leading approaches exist to making laser-based neutron sources. The first is to irradiate a sample of material rich in deuterium (and possibly tritium or $^3$He), raising the target to a high enough temperature to induce fusion reactions (Toupin *et al.*, 2001; Izumi *et al.*, 2002; Karsch *et al.*, 2003; Davis & Petrov, 2008; Bang *et al.*, 2013) This leads to an isotropic source of nearly monochromatic neutrons, though relatively low yields ($\sim 10^7$ n, or $\sim 10^6$ n/sr). Alternatively, laser-accelerated ion beams can be directed into a converter composed of lithium or beryllium (Davis *et al.*, 2010), a "pitcher–catcher" configuration, to induce neutron-producing nuclear reactions, such as various p-Li, d-Li, d-Be channels. The resulting neutrons from these direct nuclear reactions will, as a consequence of kinematics, be dominantly forward-directed. This has potential advantages, as reducing the solid angle over which the neutrons are emitted can lead to increased neutron fluences (in n/sr) and reduced needs for shielding. Early experiments in laser-based neutron sources (Lancaster *et al.*, 2004; Higginson *et al.*, 2010, 2011) used ions from target normal sheath acceleration (TNSA) (Hatchett *et al.*, 2000; Maksimchuk *et al.*, 2000; Snavely *et al.*, 2000; Hegelich *et al.*, 2002, 2006; Roth *et al.*, 2002) whereby an intense ($I > 10^{18}$W/cm$^2$) laser pulse incident on a $\sim$10 μm thick foil generates an electrostatic sheath on the rear of the foil that acts as a virtual cathode and accelerates the ions.

Recent experiments have shown dramatic improvement to laser-based neutron source yields (Jung *et al.*, 2013*a*; Roth *et al.*, 2013, 2016; Favalli *et al.*, 2016*b*) through the application of "next-generation," ion acceleration mechanisms. In these experiments, an acceleration mechanism called the "break-out afterburner" (BOA) was employed that relies on laser–plasma dynamics occurring during relativistic-induced transparency (RIT) in thin ($\sim$100 nm thickness) targets (Yin *et al.*, 2006, 2007; Henig *et al.*, 2009; Palaniyappan *et al.*, 2012; Hegelich *et al.*, 2013; Jung *et al.*, 2013*b*, *c*, 2015*a*, *b*). While such thin targets do not survive interaction with the prepulses and pedestal of a typical high-intensity high-power short-pulse laser, laser systems such as the LANL Trident laser (Batha *et al.*, 2008) have been modified for high pulse contrast (Shah *et al.*, 2009) making the BOA possible. Unlike TNSA, in the BOA the predominant ion acceleration occurs *volumetrically* in the target in regions of highest electron density during RIT. By choosing a deuterated laser target material such that ionic species separation prior to the onset of RIT is modest, the peak longitudinal electric field in the target can be made to coincide with the locations of the deuterons, allowing the BOA process to accelerate them to high energy (>100 MeV) efficiently. Recent experiments demonstrated this by using the high-contrast Trident short-pulse beam with plastic ($CH_2$) and deuterated plastic ($CD_2$) target foils of a range of thicknesses and a copper-shielded beryllium converter to produce neutrons from the ion beams through deuteron breakup, (d,n), and (p,n) reactions in the converter. With thin targets (400 nm $CD_2$) in the BOA acceleration regime, record neutron yields ($\sim 5 \times 10^9$ n/sr in a $\sim$ns pulse width) and energies (up to $\sim$ 80 MeV) were measured (Roth *et al.*, 2013); a subsequent campaign with an improved tungsten-beryllium converter improved upon these yields ($\sim 2 \times 10^{10}$ n/sr) (Favalli *et al.*, 2014) [Davis & Petrov (2008) reported neutron yields in their



CAMBRIDGE UNIVERSITY PRESS

simulations of up to $10^7$ neutrons per Joule of laser energy. Experiments on Trident exploiting the BOA produced more than twice that yield (Roth *et al.*, 2013).]

In this paper, we revisit BOA laser-based neutron sources and examine using VPIC kinetic plasma simulations (Bowers *et al.*, 2008*a*, *b*, 2009) the advantages in terms of neutron yields and spectra of using different laser target materials.

## Kinetic modeling of laser-ion acceleration and neutron production from $CD_2$ targets

We model the relativistic laser–plasma interaction in a manner that has been validated with past Trident laser experiments in the BOA regime (Hegelich *et al.*, 2013). Specifically, we employ a uniform, two-dimensional (2D), Cartesian mesh with a domain of size 100 μm in $x$ (longitudinally) by 45 μm in $z$ (transversely) with absorbing particle and field boundary conditions. The laser is an $S$-polarized (i.e., laser electric field polarized along $y$) Gaussian beam of wavelength 1.0 μm launched from the left of the domain with a peak field $a_0 \equiv eE_0/m_e\omega_0 c = 10.4$ ($I_0 = 3.3 \times 10^{20}$ W/cm$^2$) with laser electric field profile at best focus $E_y \sim \exp(-z^2/w^2)$ with $w = 5.12$ μm. This choice of polarization has been shown to provide a closer match in both timing of onset of relativistic transparency and ion beam energy to 3D simulations than 2D $P$-polarization (Stark *et al.*, 2017). A sine-squared temporal envelope $I(t) = I_0 \sin^2(t\pi/\tau)$ is employed, where $\tau = 2 \times \text{FWHM} = 1080$ fs. For these laser parameters, the incident laser power is $P(t) = 2\pi I_{\max}(t) \int_0^\infty r \exp(-2r^2/w^2) dr = (\pi/2) w^2 I_{\max}(t)$ where $I_{\max}$ is the laser intensity on axis. The incident laser energy is $\mathcal{E} = \int dt\, P(t) = (\pi/4)\tau w^2 I_0 \sim 73$ J, comparable to the 70–80 J of energy available in a typical pulse from the C (short pulse) beam of the Trident laser. The target foil is placed 10 μm from the left simulation boundary and has initial thickness 240 nm and density $\rho = 1.02 \text{g/cm}^3$ (electron density $n_{e0} = 280 n_{\text{cr}}$, where $n_{\text{cr}} = m_e\omega_0^2/4\pi e^2$ is the critical density for a laser of angular frequency $\omega_0$). The plasma is taken to be fully ionized with 2800 particles/cell/species and initial temperatures $T_e = 100$ keV and $T_i = 10$ eV for both ionic species. Realistic mass ratios are used for electrons and ions. The simulation domain is $50{,}000 \times 9000$ cells, sufficient to resolve both initial skin depth $\delta^0 = c/\omega_{\text{pe}}^0$ and Debye length $\lambda_{\text{De}}^0 = [k_B T_e^0/4\pi n_e^0 e^2]^{1/2}$: $\delta^0 \approx 5\Delta x$, $\delta^0 \approx 2\Delta z$, $\lambda_{\text{De}}^0 \approx 2\Delta x$, and $\lambda_{\text{De}}^0 \approx 1\Delta z$, where $\Delta x$ and $\Delta z$ are the mesh sizes in $x$ and $z$, respectively, and superscripts "0" denote quantities at $t = 0$. We run our simulations until the laser has left the simulation volume ($t = 1400$ fs).

In Figure 1, we show contour plots of carbon (left) and deuteron (right) ion energy at three different times. The top panels are at time 491.7 fs, near the onset of RIT. The center panels are at intermediate time 793.1 fs and the bottom panels are at time 1348.2 fs, near the end of the simulation, when most of the ion acceleration has occurred. The colors denote ion kinetic energy per nucleon. As the BOA progresses, the most energetic

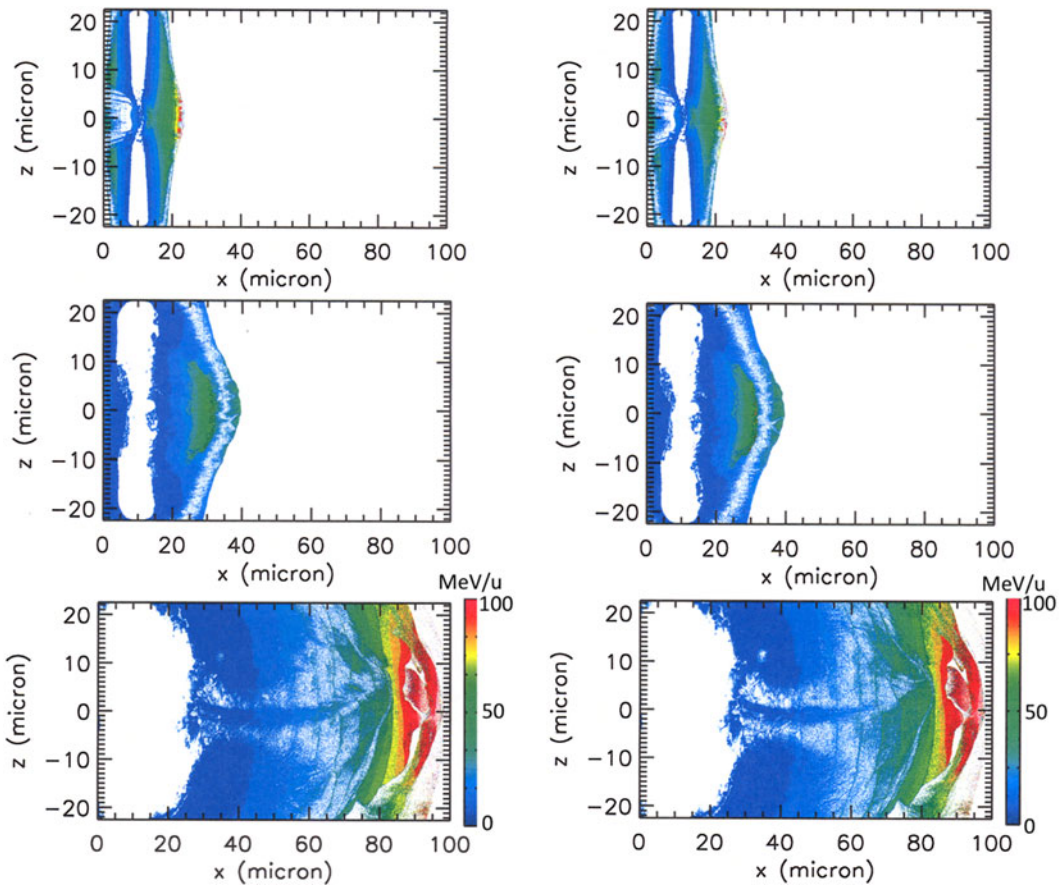


**Fig. 1.** Spatial profiles of carbon (left) and deuteron (right) energy per nucleon from simulations of BOA acceleration of ions in a $CD_2$ laser target. Shown are profiles around the time of the onset of RIT (top panels), a time mid-way through the acceleration (center panels), and at the end of the RIT phase (bottom panels), when most of the ion acceleration has occurred. The colors indicate relative ion kinetic energy per nucleon at each time shown; for the bottom two panels, an absolute scale of ion energy per nucleon is indicated by the color bars.

https://doi.org/10.1017/S0263034617000908 Published online by Cambridge University Press

ions are found near the right of the simulation domain. Note that because the two ionic species have the same charge-to-mass ratios, the kinematics of the deuterons and carbon ions are identical and, not surprisingly, the two accelerate with identical spatial and energy profiles. In the left panel of Figure 2, we show energy spectra of carbon ions (black) and deuterons (red) at time 1348.2 fs in a 1 μm cut through the center of the simulation domain and the two ion species indeed possess identical spectra (to within statistical error inherent with the particle-in-cell algorithm.)

As discussed Roth *et al.* (2013) and Favalli *et al.* (2014), this beam of laser-generated ions can be directed into a beryllium converter in a pitcher–catcher neutron source configuration to sample a variety of neutron-producing nuclear processes. We now consider alternative laser target options for neutron production chosen according to the following criteria: (1) the target must be "deuteron rich," meaning a high mass fraction of deuterium within the bulk target plasma, (2) the charge-to-mass ratios of the non-deuteron ions in the bulk target plasma must be comparable (though not necessarily identical) to that of the deuterons, and (3) the target must be sufficiently thin that the BOA occurs with the onset of RIT near the peak intensity of the laser pulse. The first criterion, not surprisingly, ensures that the acceleration of deuterons will be efficient, as the higher the mass fraction $f_D$ of deuterons in the target, defined as $f_D = m_D n_D / \sum_i m_i n_i$ where $m_i$ and $n_i$ are the masses and number densities of atoms of species $i$ in the targets, the larger the fraction of laser energy that will go into acceleration of deuterons as opposed to other species. [This is somewhat analogous to a published effect of increased proton density in TNSA (Robinson *et al.*, 2006).] The second ensures incomplete species separation from electrostatic fields in the target prior to the onset of RIT. As discussed by Yin *et al.* (2007) and inferred experimentally (Jung *et al.*, 2013*c*), the presence of dissimilar charge-to-mass ratio species can lead to species stratification as the higher charge-to-mass species under the laser spot are expelled from the target, moving away from the target in the direction of the laser propagation and leaving behind lower charge-to-mass species to receive most of the acceleration from the laser. If the expelled ions are deuterons ($Z^*/A = 1/2 = 0.5$), as might be expected for, for example, a deterium-loaded palladium target ($Z^*/A \sim 25/106 = 0.24$ for initiating RIT using Trident-like parameters), the peak electrostatic field would likely preferentially accelerate the heavier palladium ions, with the deuterons accelerated only indirectly through inertial tamping of the primary species [as with the protons in Jung *et al.* (2013*c*)]. Note that this expulsion of high charge-to-mass ratio is not always complete, particularly when high concentrations of these ions are present in the bulk. This was the explanation provided and later confirmed in kinetic simulations for the high proton energies measured in the experiments of Hegelich *et al.* (2013) and Jung *et al.* (2015*b*) (a feature of the dynamics that we will exploit shortly). The final criterion ensures that BOA acceleration dominates. The BOA has been shown to be robust experimentally, provided one has sufficient laser pulse contrast, and couples a large fraction of the laser beam energy into the ions (Jung *et al.*, 2013*b*).

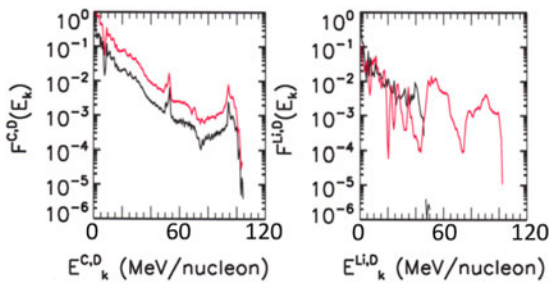


**Fig. 2.** Ion energy spectra of carbon ions (black) and deuterons (red) from simulations of BOA acceleration of ions in a $CD_2$ laser target at time 1348.2 fs (left). Spectra for $^7$Li ions (black) and deuterons (red) from simulations of BOA acceleration of ions in a $^7$LiD laser target at time 1341.6 fs (right). In both cases, shown are data binned within a 1 μm-wide cut through the center of the simulation domain. In $CD_2$, the two ion species have the same charge-to-mass ratios, so they possess nearly identical spectra. In $^7$LiD, the energy spectra of deuterons have a preponderance of ions at high energy (>50 MeV/nucleon) as a result of species-separation kinematics during BOA acceleration.

## Alternate target materials

To compare neutron yields from different target materials in our study, we keep the laser parameters fixed and choose our target thicknesses in our simulations in such a manner that the areal density of electrons beneath the laser spot is held constant, equal to that of a reference, solid-density, $CH_2$ target foil ($n_e/n_{cr} = 280$), the optimal target thickness with the laser parameters given above having been found to be 240 nm from prior studies. In practice, this prescription leads to reasonably accurately estimates of the target thicknesses yielding BOA ion beams with maximal energies. The parameters for the targets in our study are given in Table 1. With the exception of $^7$LiD, the target materials' ions have identical charge-to-mass ratios. Consequently, the deuterons and the other ions ($^6$Li, $^{12}$C, $^{14}$N) accelerate as in Figure 1, with nearly identical spatial and energy profiles for the different ion species, with profiles qualitatively similar to those shown in Figure 1. However, this is not so for $^7$LiD, for which the deuterons have slightly larger charge-to-mass ratios than the $^7$Li ions. As shown in Figure 3, the ion species separate prior to RIT (see the top panel). As BOA acceleration proceeds, the fastest deuterons continue to propagate ahead of the $^7$Li ions (see the middle and lower panels). This results in a preponderance of deuterons at higher energies, evident in the energy spectra in the right panel of Figure 2, where energy spectra of $^7$Li (black) and deuterium (red) are shown from a 1 μm wide

**Table 1.** Simulation parameters and yields for different target materials. A 240 nm deuterated plastic $^{12}CD_2$ target serves as a reference; other materials have comparable or larger deuteron mass fractions $f_D$. Target thicknesses $w$ were selected to have the same electron areal density as the reference. $Y_{d,rel}$ is the relative number of deuterons entering the Be converter. Relative neutron yield $Y_{n,rel} \equiv Y_n / Y_{n,CD_2}$ ($Y_n$ and $Y_{n,CD_2}$ are neutrons per source deuteron for target and reference materials, respectively) are obtained from MCNP 6.1.1 tallies of neutron leakage from a 16.5 cm wide, 1 cm radius Be cylinder with point sources of deuterons directed along the axis at base of the cylinder with spectra obtained from VPIC calculations. The first three targets are solid at room temperature; the latter two require cryogenic conditions

| Material | $w$ (nm) | ρ (g/cm$^3$) | $f_D$ | $n_e/n_{cr}$ | $Y_{d,rel}$ | $Y_{n,rel}$ |
|---|---|---|---|---|---|---|
| $^{12}CD_2$ | 240 | 1.02 | 0.25 | 280 | 1.00 | 1.0 |
| $^7$LiD | 300 | 0.942 | 0.22 | 226 | 1.09 | 3.9 |
| $^6$LiD | 300 | 0.837 | 0.25 | 226 | 1.21 | 2.0 |
| $^{14}ND_3$ | 255 | 0.961 | 0.30 | 263 | 1.17 | 1.4 |
| $^{12}CD_4$ | 463 | 0.529 | 0.40 | 145 | 2.13 | 2.9 |

https://doi.org/10.1017/S0263034617000908 Published online by Cambridge University Press

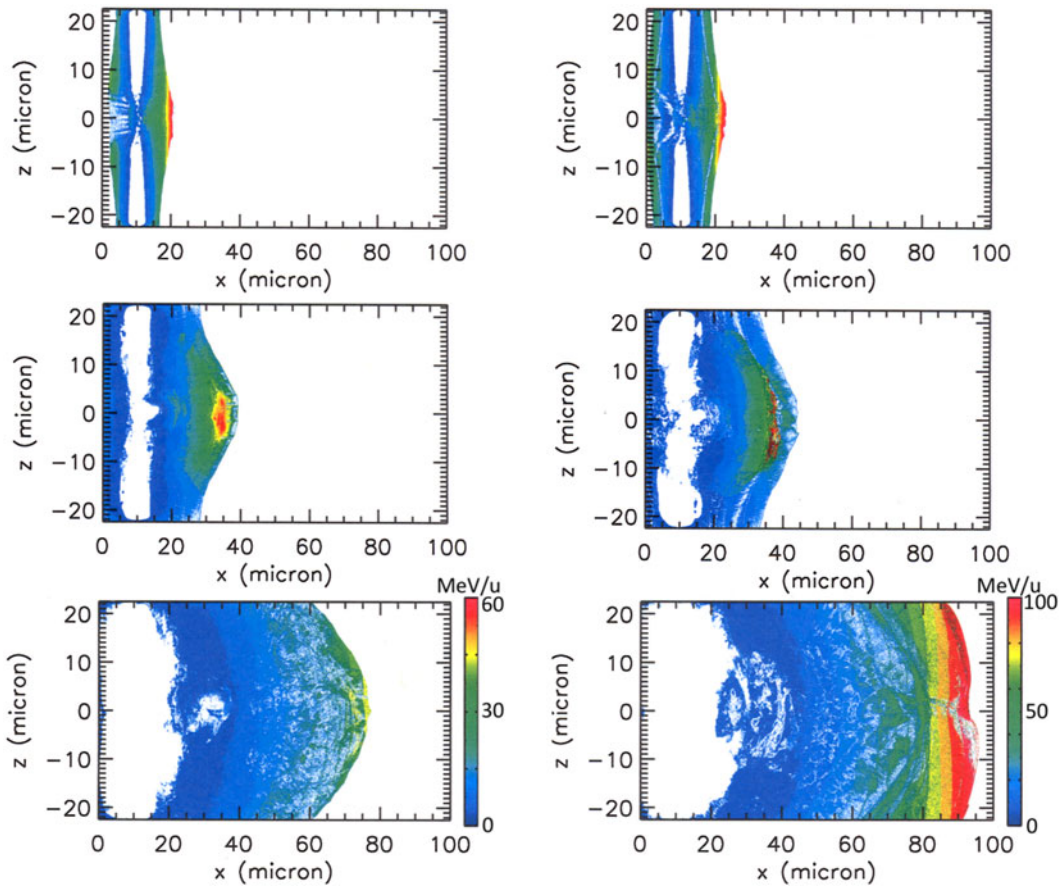


**Fig. 3.** Spatial profiles of $^{7}$Li (left) and deuteron (right) energy per nucleon from simulations of BOA acceleration of ions in a $^{7}$LiD laser target. Shown are profiles at $t = 494$ fs, around the time of the onset of RIT (top panels); $t = 883$ fs, mid-way through the acceleration (center panels); and at $t = 1342$ fs, near the end of the RIT phase (bottom panels) when most of the ion acceleration has occurred. The colors indicate relative ion kinetic energy per nucleon at each time shown; for the bottom two panels, an absolute scale of ion energy per nucleon is indicated by the color bars.

cut through the center of the simulation volume at time 1341.6 fs, near the end of the RIT phase when most of the ion acceleration has taken place.

Relative to the $^{12}CD_2$ reference case, the VPIC simulations reveal two different approaches to increasing neutron yield: The first is to use a target material such as deuterated methane or ammonia with the same $Z^*/A = 0.5$ as deuterium but a higher mass fraction of deuterons ($f_D = 0.30$ and 0.40 for deuterated ammonia and methane, respectively). Such targets couple a larger fraction of laser energy into the deuterons as opposed to the other ions. The second is to use a target such as $^{7}$LiD which, despite a lower $f_D$ than the reference $^{12}CD_2$ target, nevertheless has higher mean deuteron energy. Higher energy deuterons have longer stopping ranges in the converter and may sample higher cross-sections for some neutron-producing nuclear reactions. Both increase neutron yield per deuteron over the $^{12}CD_2$ reference case.

To compare neutron production from the different ion beams via the multiple primary [deuteron breakup, (d,n), etc.] and secondary [(p,n), e.g.] processes within the converter, we used the Monte Carlo N-Particle Transport code (MCNP version 6.1.1) (Werner 2017). The neutron beryllium converter was modeled as (1) 16.5 cm and (2) 4 mm long, 1 cm radius beryllium cylinders of density 1.85 g/cm$^3$. The incident deuteron source was a parallel beam directed toward the base of the cylinder along the axis with energy spectra obtained from VPIC calculations. The lengths of the converters were chosen as follows: the 16.5 cm length (case 1) exceeds the stopping range of the highest energy deuterons in the simulations (260 MeV from the $^{7}$LiD targets, with a range of 16.2 cm as calculated by the Stopping and Range of Ions in Matter (SRIM) code (Ziegler *et al.*, 2010); the 4 mm length (case 2) is the stopping range of the mean-energy (33 MeV) deuterons from the $^{7}$LiD spectra. The neutron production was tallied in two ways: as total neutron leakage over the converter surface or as forward-directed neutrons emitted (leaked) in a cone of half-angle 24° centered in the base of the cylinder where the deuterons impinge upon the converter. [This angle was chosen because for a deuteron of energy 33 MeV, 24° is the half-width of the angular distribution of neutrons produced by deuteron stripping (Serber, 1947).] The neutron production was tallied by means of the F1 Tally from $2 \times 10^9$ source deuterons sampled from the respective calculated VPIC energy spectra. ENDF/B-VII cross-section tables (Chadwick *et al.*, 2006, 2011) were used for neutrons with energy below 20 MeV and protons with energy below 113 MeV. An improved version of the Cascade-Exciton Model (CEM3.03) was used for higher energy reactions. The Los Alamos Quark Gluon String Model (LAQGSM3.03) (Mashnik *et al.*, 2005) as implemented in MCNP version 6.1.1, was also used at all energies for heavy and light ion interactions. The calculated neutron energy spectra resulting from each of the deuteron distributions multiplied by the relative deuteron yield in each ion spectra are shown in

https://doi.org/10.1017/S0263034617000908 Published online by Cambridge University Press

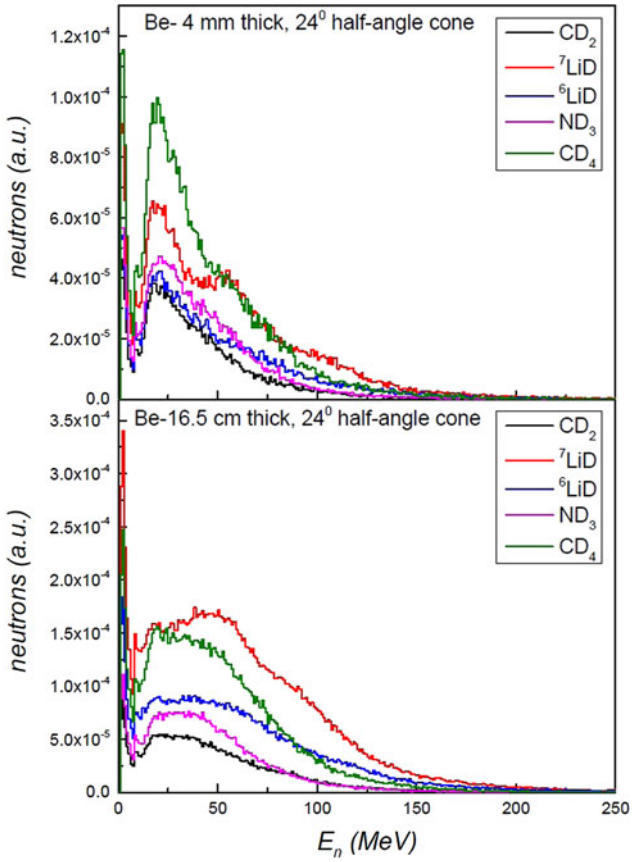


**Fig. 4.** Neutron spectra obtained from MCNP modeling of a point source of deuterons with energy spectra from VPIC simulations initiated along the axis at the base of 4 mm (top) and 16.5 cm wide (bottom), 1 cm radius beryllium cylinders. Tallied are neutron leakages from the converters. Note that for the 16.5 cm converter, $^{7}$LiD generates the most neutrons, particularly at high energy ($E_n > 25$MeV), whereas for the thinner converters, $CD_4$ produces the most neutrons.

Figure 4. In Table 1, we report comparisons of total neutron yield for the 16.5 cm converter. The $^{7}$LiD target produces nearly four times as many neutrons as a $^{12}CD_2$ target; similarly, the forward neutron production with the $^{7}$LiD target was calculated to be 4.3 times higher than with the $^{12}CD_2$ reference target.

## Conclusions

In summary, we have modeled several variations of neutron sources based upon the pitcher–catcher concept using the BOA mechanism to accelerate ions. Our simulations point to two approaches to enhancing neutron yield through choice of laser target materials: use of targets composed of materials with higher fractional mass densities of deuterons and the use of targets that, inherent to the kinematics of the BOA mechanism, lead to higher deuteron energies and thus higher neutron yields. Several candidate target materials have been identified and assessed for Trident-like laser parameters that appear promising for increasing neutron yield relative to the present state of the art, which employed $CD_2$ targets on the Trident laser system. While our study has focused on Trident-like conditions and, as the Trident laser is in the process of decommission and re-siting elsewhere, therefore our specific simulated parameters may not be directly applicable to other systems, we nevertheless expect that the dynamics we report upon will be applicable to other high-contrast, high-power, short-pulse laser systems. We also showed that neutron spectra can also be controlled in these experiments. For instance, the use of a laser target such as $^{7}$LiD generates a hardened neutron spectrum, that is, a preponderance of neutrons at higher energy, which would be of value for applications requiring enhanced neutron penetrability, for example, active neutron interrogation in shielded material. While we recognize that $^{7}$LiD poses challenges for target fabrication, other target materials (e.g., $^{13}CD_2$ plastic or $^{18}OD_2$ ice) have $f_D$ and $Z^*/A$ ratio properties similar to those of $^{7}$LiD and should evince similar advantages. Finally, as evidenced by the results of a 4 mm thick converter (the top panel of Fig. 4), we note that according to application needs, converter geometry and target material can be optimized to balance possibly conflicting requirements on neutron yield and neutron energy spectra.

Work performed under the auspices of the US Department of Energy by the Los Alamos National Security, LLC Los Alamos National Laboratory under contract DE-AC52-06NA25396. This work was supported by the LANL LDRD program. Computing time on the ASC Cielo machine was provided by Capability Class Computing allocations. The authors wish to acknowledge useful discussions with Juan Fernández, Martyn Swinhoe, D. Cort Gautier, B. Manuel Hegelich, John Hendricks, and Markus Roth. Apollo Albright assisted in preparing the data.

## References

**Alvarez J, Fernández-Tobias J, Mima K, Nakai S, Kar S, Kato Y and Perlado JM** (2014) Laser driven neutron sources: characteristics, applications and prospects. *Physics Procedia* **60**, 29–38.

**Bang W, Barbui M, Bonasera A, Dyer G, Quevedo HJ, Hagel K, Schmidt K, Consoli F, De Angelis R, Andreoli P, Gaul E, Bernstein AC, Donovan M, Barbarino M, Kimura S, Mazzocco M, Sura J, Natowitz JB and Ditmire T** (2013) Temperature measurements of fusion plasmas produced by petawatt-laser-irradiated $D_2$–$^{3}$He or $CD_4$–$^{3}$He clustering gases. *Physical Review Letters* **111**, 055002.

**Batha SH, Aragonez R, Archuleta FL, Archuleta TN, Benage JF, Cobble JA, Cowan JS, Fatherley VE, Flippo KA, Gautier DC, Gonzales RP, Greenfield SR, Hegelich BM, Hurry TR, Johnson RP, Kline JL, Letzring SA, Loomis EN, Lopez FE, Luo SN, Montgomery DS, Oertel JA, Paisley DL, Reid SM, Sanchez PG, Seifter A, Shimada T and Workman JB** (2008) TRIDENT high-energy-density facility experimental capabilities and diagnostics. *The Review of Scientific Instruments* **79**(10), 10F305.

**Bowers KJ, Albright BJ, Yin L, Bergen B and Kwan TJT** (2008*a*) Ultrahigh performance three-dimensional electromagnetic relativistic kinetic plasma simulation). *Physics of Plasmas* **15**(5), 055703.

**Bowers KJ, Albright BJ, Bergen B, Yin L, Barker KJ and Kerbyson DJ** (2008*b*) 0.374 Pflop/s trillion-particle kinetic modeling of laser plasma interaction on Roadrunner. In *Proceedings of the 2008 ACM/IEEE Conference on Supercomputing*. IEEE Press, pp. 63–74.

**Bowers KJ, Albright BJ, Yin L, Daughton W, Roytershteyn V, Bergen B and Kwan TJT** (2009) Advances in petascale kinetic plasma simulation with VPIC and Roadrunner. *Journal of Physics: Conference Series* **180**(1), 012055.

**Buffler A** (2004) Contraband detection with fast neutrons. *Radiation Physics and Chemistry* **71**, 853–861.

**Chadwick MB, Herman M, Obložinský P, Herman M, Greene NM, McKnight RD, Smith DL, Young PG, MacFarlane RE, Hale GM, Frankle SC, Kahler AC, Kawano T, Little RC, Madland DG, Moller P, Mosteller RD, Page PR, Talou P, Trellue H, White MC, Wilson WB, Arcilla R, Dunford CL, Mughabghab SF, Pritychenko B, Rochman D, Sonzogni AA, Lubitz CR, Trumbull TH, Weinman JP, Brown DA, Cullen DE, Heinrichs DP, McNabb DP, Derrien H, Dunn ME, Larson NM, Leal LC, Carlson AD, Block RC, Briggs JB, Cheng ET, Huria HC, Zerkle ML, Kozier KS, Courcelle A, Pronyaev V and van**

https://doi.org/10.1017/S0263034617000908 Published online by Cambridge University Press

**der Marck SC** (2006) Evaluated nuclear data file ENDF/B-VII.0ENDF/B-VII.0: next generation evaluated nuclear data library for nuclear science and technology. *Nuclear Data Sheets* **107**(12), 2931–3060.

**Chadwick MB, Herman M, Obložinský P, Dunn ME, Danon Y, Kahler AC, Smith DL, Pritychenko B, Arbanas G, Arcilla R, Brewer R, Brown DA, Capote R, Carlson AD, Cho YS, Derrien H, Guber K, Hale GM, Hoblit S, Holloway S, Johnson TD, Kawano T, Kiedrowski BC, Kim H, Kunieda S, Larson NM, Leal L, Lestone JP, Little RC, McCutchan EA, MacFarlane RE, MacInnes M, Mattoon CM, McKnight RD, Mughabghab SF, Nobre GPA, Palmiotti G, Palumbo A, Pigni MT, Pronyaev VG, Sayer RO, Sonzogni AA, Summers NC, Talou P, Thompson IJ, Trkov A, Vogt RL, van der Marck SC, Wallner A, White MC, Wiarda D and Young PG** (2011) Special issue on ENDF/B-VII.1 LibraryENDF/B-VII.1 nuclear data for science and technology: cross sections, covariances, fission product yields and decay data. *Nuclear Data Sheets* **112**(12), 2887–2996.

**Davis J and Petrov GM** (2008) Angular distribution of neutrons from high-intensity laser–target interactions. *Plasma Physics and Controlled Fusion* **50**(6), 065016.

**Davis J, Petrov GM, Petrova T, Willingale L, Maksimchuk A and Krushelnick K** (2010) Neutron production from $^{7}$Li(d, xn) nuclear fusion reactions driven by high-intensity laser-target interactions. *Plasma Physics and Controlled Fusion* **52**(4), 045015.

**Favalli A, Mehner HC, Crochemore JM and Pedersen B** (2009) Pulsed neutron facility for research in illicit trafficking and nuclear safeguards. *IEEE Transactions on Nuclear Science* **56**(3), 1292–1296.

**Favalli A, Aymond F, Bridgewater JS, Croft S, Deppert O, Devlin MJ, Falk K, Fernández JC, Gautier DC, Gonzales MA, Goodsell AV, Guler N, Hamilton CE, Hegelich BM, Henzlova D, Ianakiev KD, Iliev M, Johnson RP, Jung D, Kleinschmidt A, Koehler KE, Pomerantz I, Roth M, Santi PA, Shimada T, Swinhoe MT, Taddeucci TN, Wurden GA, Palaniyappan S and McCary E** (2014) Nuclear material detection by one-short-pulse-laser-driven neutron source. In *IEEE Nuclear Symposium*, Seattle, USA.

**Favalli A, Bridgwater J, Croft S, Falk K, Fernández JC, Gautier D, Guler N, Hamilton C, Henzlova D, Ianakiev KD, Iliev M, Johnson RP, Jung D, Roth M, Shimada T and Swinhoe M** (2016*a*) Laser-driven neutron source for detection of nuclear material. In *Proceedings of the* 2016 *Advances in Nuclear Nonproliferation Technology and Policy Conference*, Santa Fe, NM, USA, 25–30 Sept.

**Favalli A, Guler N, Henzlova D, Falk K, Croft S, Gautier DC, Ianakiev K, Iliev M, Palaniyappan S, Roth M, Fernández J and Swinhoe M** (2016*b*) Experimental observation of β-delayed neutrons from $^{9}$Li as a way to study short-pulse laser-driven deuteron production. arXiv:1605.05702v1 [physics.plasm-ph].

**Hatchett SP, Brown CG, Cowan TE, Henry EA, Johnson JS, Key MH, Koch JA, Langdon AB, Lasinski BF, Lee RW, Jackinnon AJ, Pennington DM, Perry MD, Phillips TW, Roth M, Sangster TC, Singh MS, Snavely RA, Stoyer MA, Wilks SC and Yasuike K** (2000) Electron, photon, and ion beams from the relativistic interaction of petawatt laser pulses with solid targets. *Physics of Plasmas* **7**(5), 2076–2082.

**Hegelich BM, Albright BJ, Cobble J, Flippo K, Letzring S, Paffett M, Ruhl H, Schreiber J, Schulze RK and Fernández JC** (2006) Laser acceleration of quasi-monoenergetic MeV ion beams. *Nature* **439**(7075), 441–444.

**Hegelich BM, Jung D, Albright BJ, Cheung M, Dromey B, Gautier DC, Hamilton C, Letzring S, Munchhausen R, Palaniyappan S, Shah R, Wu H-C, Yin L and Fernández JC** (2013) 160 MeV laser-accelerated protons from CH2 nano-targets for proton cancer therapy. arXiv:1310.8650 [physics.plasm-ph].

**Hegelich M, Karsch S, Pretzler G, Habs D, Witte K, Guenther W, Allen M, Blazevic A, Fuchs J, Gauthier JC, Geissel M, Audebert P, Cowan T and Roth M** (2002) MeV ion jets from short-pulse-laser interaction with thin foils. *Physical Review Letters* **89**(8), 085002.

**Henig A, Kiefer D, Markey K, Gautier DC, Flippo KA, Letzring S, Johnson RP, Shimada T, Yin L, Albright BJ, Bowers KJ, Fernández JC, Rykovanov SG, Wu H-C, Zepf M, Jung D, Liechtenstein VK, Schreiber J, Habs D and Hegelich BM** (2009) Enhanced laser-driven ion acceleration in the relativistic transparency regime. *Physical Review Letters* **103**(4), 045002.

**Higginson DP, McNaney JM, Swift DC, Bartal T, Hey DS, Kodama R, Le Pape S, Mackinnon A, Mariscal D, Nakamura H, Nakanii N, Tanaka KA and Beg FN** (2010) Laser generated neutron source for neutron resonance spectroscopy. *Physics of Plasmas* **17**, 100701.

**Higginson DP, McNaney JM, Swift DC, Petrov GM, Davis J, Frenje JA, Jarrott LC, Kodama R, Lancaster KL, Mackinnon AJ, Nakamura H, Patel PK, Tynan G and Beg FN** (2011) Production of neutrons up to 18 MeV in high-intensity, short-pulse laser matter interactions. *Physics of Plasmas* **18**(10), 100703.

**Izumi N, Sentoku Y, Habara H, Takahashi K, Ohtani F, Sonomoto T, Kodama R, Norimatsu T, Fujita H, Kitagawa Y, Mima K, Tanaka KA, Yamanaka T** (2002) Observation of neutron spectrum produced by fast deuterons via ultraintense laser plasma interactions. *Physical Review E* **65**, 036413.

**Jung D, Falk K, Guler N, Deppert O, Devlin M, Favalli A, Fernández JC, Gautier DC, Geissel M, Haight R, Hamilton CE, Hegelich BM, Johnson RP, Merrill F, Schaumann G, Schoenberg K, Schollmeier M, Shimada T, Taddeucci T, Tybo JL, Wender SA, Wilde CH, Wurden GA and Roth M** (2013*a*) Characterization of a novel, short pulse laser-driven neutron source. *Physics of Plasmas* **20**(5), 056706.

**Jung D, Yin L, Albright BJ, Gautier DC, Letzring S, Dromey B, Yeung M, Hörlein R, Shah R, Palaniyappan S, Allinger K, Schreiber J, Bowers KJ, Wu H-C, Fernández JC, Habs D and Hegelich BM** (2013*b*) Efficient carbon ion beam generation from laser-driven volume acceleration. *New Journal of Physics* **15**(2), 023007.

**Jung D, Yin L, Gautier DC, Wu HC, Letzring S, Dromey B, Shah R, Palaniyappan S, Shimada T, Johnson RP, Schreiber J, Habs D, Fernández JC, Hegelich BM and Albright BJ** (2013*c*) Laser-driven 1 GeV carbon ions from preheated diamond targets in the break-out afterburner regime. *Physics of Plasmas* **20**(8), 083103.

**Jung D, Albright BJ, Yin L, Gautier DC, Dromey B, Shah R, Palaniyappan S, Letzring S, Wu H-C, Shimada T, Johnson RP, Habs D, Roth M, Fernández JC and Hegelich BM** (2015*a*) Scaling of ion energies in the relativistic-induced transparency regime. *Laser and Particle Beams* **33**(4), 695–703.

**Jung D, Senje L, McCormack O, Yin L, Albright BJ, Letzring S, Gautier DC, Dromey B, Toncian T, Fernández JC, Zeph M and Hegelich BM** (2015*b*) On the analysis of inhomogeneous magnetic field spectrometer for laser-driven ion acceleration. *Review of Scientific Instruments* **86**(3), 033303.

**Karsch S, Düsterer S, Schwoerer H, Ewald F, Habs D, Hegelich M, Pretzler G, Pukhov A, Witte K and Sauerbrey R** (2003) High-intensity laser induced ion acceleration from heavy-water droplets. *Physical Review Letters* **91**, 015001.

**Lancaster KL, Karsch S, Habara H, Beg FN, Clark EL, Freeman R, Key MH, King JA, Kodama R, Krushelnick K, Ledingham KWD, McKenna P, Murphy CD, Norreys PA, Stephens R, Stöeckl C, Yotama Y, Wei MS and Zeph M** (2004) Characterization of $^{7}$Li(p, n)$^{7}$Be neutron yields from laser produced ion beams for fast neutron radiography. *Physics of Plasmas* **11**, 3404–3408.

**Ma J, Delaire O, May AF, Carlton CE, McGuire MA, VanBebber LH, Abernathy DL, Ehlers G, Hong T, Huq A, Tian W, Keppens VM, Shao-Horn Y and Sales BC** (2013) Glass-like phonon scattering from a spontaneous nanostructure in $AgSbTe_2$. *Nature Nanotechnology* **8**, 445–451.

**Maksimchuk A, Gu S, Flippo K, Umstadter D and Bychenkov VY** (2000) Forward ion acceleration in thin films driven by a high-intensity laser. *Physical Review Letters* **84**(18), 4108–4112.

**Mashnik SG, Baznat MI, Gudima KK, Sierk AJ and Prael RE** (2005) CEM03 and LAQGSM03: extension of the CEM2k+ GEM2 and LAQGSM codes to describe photo-nuclear reactions at intermediate energies (30 MeV to 1.5 GeV). *Journal of Nuclear and Radiochemical Sciences* **6**(2), A1–A19.

**Palaniyappan S, Hegelich BM, Wu HC, Jung D, Gautier DC, Yin L, Albright BJ, Johnson RP, Shimada T, Letzring S, Offermann DT, Ren J, Huang C-K, Hörlein R, Dromey B, Fernández JC and Shah RC** (2012) Dynamics of relativistic transparency and optical shuttering in expanding overdense plasmas. *Nature Physics* **8**(10), 763–769.

https://doi.org/10.1017/S0263034617000908 Published online by Cambridge University Press

**Perkins LJ, Logan BG, Rosen MD, Perry MD, Diaz de la Rubia T, Ghoniem NM, Ditmire T, Springer PT and Wilks SC** (2000) The investigation of high intensity laser driven micro neutron sources for fusion materials research at high fluence. *Nuclear Fusion* **40**, 1–19.

**Robinson AL, Bell AR and Kingham RJ** (2006) Effect of target composition on proton energy spectra in ultraintense laser-solid interactions. *Physical Review Letters* **96**(3), 035005.

**Roth M, Blazevic A, Geissel M, Schlegel T, Cowan TE, Allen M, Gauthier J-C, Audebert P, Fuchs J, Meyer-ter-Vehn J, Hegelich M, Karsch S and Pukhov A** (2002) Energetic ions generated by laser pulses: a detailed study on target properties. *Physical Review Special Topics – Accelerators and Beams* **5**(6), 061002.

**Roth M, Jung D, Falk K, Guler N, Deppert O, Devlin M, Favalli A, Fernández JC, Gautier D, Geissel M, Haight R, Hamilton CE, Hegelich BM, Johnson RP, Merrill F, Schaumann G, Schoenberg K, Schollmeier M, Shimada T, Taddeucci T, Tybo JL, Wagner F, Wender SA, Wilde CJ and Wurden GA** (2013) Bright laser-driven neutron source based on the relativistic transparency of solids. *Physical Review Letters* **110**(4), 044802.

**Roth M, Jung D, Falk K, Guler N, Deppert O, Devlin M, Favalli A, Fernández JC, Gautier DC, Geissel M, Haight R, Hamilton CE, Hegelich BM, Johnson RP, Kleinschmidt A, Merrill F, Schaumann G, Schoenberg K, Schollmeier M, Shimada T, Taddeucci T, Tybo JL, Wagner F, Wender SA, Wilde CJ and Wurden GA** (2016) A bright neutron source driven by relativistic transparency of solids. *Journal of Physics: Conference Series* **688**, 012094.

**Serber R** (1947) The production of high energy neutrons by stripping. *Physical Review* **72**, 1008–1016.

**Shah RC, Johnson RP, Shimada T, Flippo KA, Fernández JC and Hegelich BM** (2009) High-temporal contrast using low-gain optical parametric amplification. *Optics letters* **34**(15), 2273–2275.

**Snavely RA, Key MH, Hatchett SP, Cowan TE, Roth M, Phillips TW, Stoyer MA, Henry EA, Sangster TC, Singh MS, Wilks SC, MacKinnon A, Offenberger A, Pennington DM, Yasuike K, Langdon AB, Lasinski BF, Johnson J, Perry MD and Campbell EM** (2000) Intense high-energy proton beams from petawatt-laser irradiation of solids. *Physical Review Letters* **85**(14), 2945–2949.

**Stark DJ, Yin L, Albright BJ and Guo F** (2017) Effects of dimensionality on kinetic simulations of laser-ion acceleration in the transparency regime. *Physics of Plasmas* **24**(5), 053103.

**Toupin C, Lefebvre E and Bonnaud G** (2001) Neutron emission from a deuterated solid target irradiated by an ultraintense laser pulse. *Physics of Plasmas* **8**(3), 1011–1021.

**Werner CJ** (2017) *MCNP Users Manual - Code Version 6.2, LA-UR-17-29981*. Los Alamos, NM: Los Alamos National Laboratory.

**Yin L, Albright BJ, Hegelich BM and Fernández JC** (2006) GeV laser ion acceleration from ultrathin targets: the laser break-out afterburner. *Laser and Particle Beams* **24**(2), 291–298.

**Yin L, Albright BJ, Hegelich BM, Bowers KJ, Flippo KA, Kwan TJT and Fernández JC** (2007) Monoenergetic and GeV ion acceleration from the laser breakout afterburner using ultrathin targets. *Physics of Plasmas* **14**(5), 056706.

**Zaccai G** (2000) How soft is a protein? A protein dynamics force constant measured by neutron scattering. *Science* **288**, 1604–1607.

**Ziegler JF, Ziegler MD and Biersack JP** (2010) SRIM – the stopping and range of ions in matter (2010). *Nuclear Instruments and Methods in Physics Research Section B: Beam Interactions with Materials and Atoms* **268**(11), 1818–1823.

https://doi.org/10.1017/S0263034617000908 Published online by Cambridge University Press